https://doi.org/10.14483/23448393.23305

Research paper

# Classification of Transient Signals Produced by Direct Impacts of a Lightning Strike on a Medium Voltage Network in the Frequency Domain Using a Deep Learning Neural Network

Clasificación de las señales transitorias producidas por el impacto directo de un rayo en una red de media tensión en el dominio de la frecuencia mediante una red neuronal de aprendizaje profundo

**Luis Eduardo Perdomo Orjuela**[1, 2, *], **Francisco Santamaria**[2], and **Nelson Enrique Vera**[2]

[1]Universidad Nacional de Colombia (Bogotá, Colombia), [2]Universidad Distrital Francisco José de Caldas (Bogotá, Colombia)
*Correspondence E-mail: leperdomoo@unal.edu.co

**Received**: March 4th, 2025
**Modified**: October 17th, 2025
**Accepted**: November 27th, 2025

## Abstract

**Context:** This research presents two main results: (i) the application of deep learning networks for the classification of transient overvoltage in the frequency domain, and (ii) the physical-mathematical formulation for the coupling of atmospheric electrical discharges in polarized media in the frequency domain.
**Method:** Initially, transient overvoltage records resulting from atmospheric electrical discharges were obtained from simulations in EMTP-ATP software, using the IEEE 13-node distribution network as a reference. Each transient overvoltage was transformed from the time domain to the frequency domain via the Fast Fourier Transform. Subsequently, the neural networks were trained, and their results were compared. For indirect lightning strikes, a complex-variable analysis of permittivity and permeability was performed. These variables were applied to the lightning coupling model in distribution lines or networks.
**Results:** Classification accuracies of 80 and 89.99% were achieved for transient overvoltage using the GoogLeNet and Python-ChatGPT neural networks, respectively. Furthermore, this work presents the coupling expression for atmospheric electrical discharges in polarized media.
**Conclusions:** The classification of transient overvoltage records using deep-layer neural networks and the physical-mathematical expression for lightning coupling in the frequency domain through complex variables allows for a broader understanding of the network response to this type of natural phenomenon.
**Keywords**: artificial intelligence, lightning, polarized media, frequency domain, deep neural networks.

https://doi.org/10.14483/23448393.23305

**Resumen**

**Contexto:** Esta investigación presenta dos resultados principales: (i) la aplicación de redes de aprendizaje profundo para la clasificación de sobretensiones transitorias en el dominio de la frecuencia y (ii) la formulación fisicomatemática para el acoplamiento de descargas eléctricas atmosféricas en medios polarizados en el dominio de la frecuencia.
**Método:** Inicialmente, se obtuvieron registros de sobretensiones transitorias producto de descargas eléctricas atmosféricas, a partir de simulaciones en el *software* EMTP-ATP, tomando como referencia la red de distribución IEEE de 13 nodos. Las sobretensiones transitorias fueron transformadas del dominio del tiempo al dominio de la frecuencia mediante la aplicación de la transformada rápida de Fourier. Posteriormente, se entrenaron las redes neuronales y se compararon sus resultados. Para descargas eléctricas por impacto indirecto, se realizó un manejo en variable compleja de la permitividad y la permeabilidad, las cuales fueron aplicadas al modelo de acoplamiento de rayos en líneas o redes de distribución.
**Resultados:** Se alcanzó una exactitud de 80 y 89.99 % en la clasificación de sobretensiones transitorias para las redes neuronales GoogLeNet y Python-ChatGPT respectivamente. Por otra parte, este trabajo presenta la expresión de acoplamiento de descargas eléctricas atmosféricas en medios polarizados.
**Conclusiones:** La clasificación de sobretensiones transitorias mediante redes neuronales de capa profunda y la expresión fisicomatemática de acoplamiento del rayo en el dominio de la frecuencia mediante variables complejas permite ampliar la comprensión de la respuesta de la red ante este tipo de fenómenos naturales.

**Palabras clave:** inteligencia artificial, descarga eléctrica atmosférica, medios polarizados, dominio de la frecuencia, redes de aprendizaje profundo

## 1. Introduction

Transient overvoltage in medium-voltage networks occurs due to direct or indirect lightning strokes [1]-[12]. Direct strokes on any phase conductors are caused by the absence of guard cables in the grid or by low-intensity lightning currents for which the attraction radius of said cables is insufficient. On the other hand, indirect strokes occur due to the coupling of the wave propagating through the air to the network. The physical-mathematical expression for this can be found in the scientific literature [13]-[24].

The classification of direct lightning strokes on medium-voltage networks allows developing appropriate investment and maintenance plans. This allows optimizing the CAPEX/OPEX of companies, utilities, and other related entities. On the other hand, improving the shielding of medium-voltage networks in rural areas, as well as implementing comprehensive lightning protection systems, has a positive impact on the service quality for end-users with sensitive loads. Improving the design of comprehensive lightning protection systems based on the characterization of surge records allows improving operation and maintenance processes, making the installation safe for network operators.

The purpose of this work is to continue with the analysis of previously conducted research detailing the composition of the IEEE 13-node test feeder, specifically the lightning current generator, the surge arresters, and the grounding system, among others [18], [25]-[30]. The second section of this article provides a brief description of said feeder in order to contextualize the progress made. GoogLeNet, Python, and ChatGPT were used to classify

https://doi.org/10.14483/23448393.23305

transient overvoltage records taken the head of the feeder (*i.e.*, on the secondary side of the 34.5/13.2 kV transformer), as presented in the third section. The reader may consult additional works conducted with artificial intelligence techniques in [13]-[16], [31]-[35]. The fourth and fifth sections detail the methodology and the analyses conducted regarding the accuracy and results obtained with our neural network-based approach. The sixth part of this research presents the physical-mathematical contribution to the coupling of atmospheric lightning discharges in polarized media. Throughout this section, the authors provide a detailed formulation of complex permittivity and permeability, together with a new proposal for its application within the Taylor model [23]. The final part of this document presents the conclusions drawn from our work.

## 2. Testing system

Our evaluation of the frequency response resulting from lightning captured at the head of the medium-voltage (MV) grid covers the frequency spectrum up to 4 kHz.

### 2.1. IEEE test feeder

The IEEE 13-node test feeder was taken as a reference to characterize the transient overvoltage resulting from direct lightning strokes in MV networks. Fig. 1 shows the system implemented in the EMTP-ATP software.

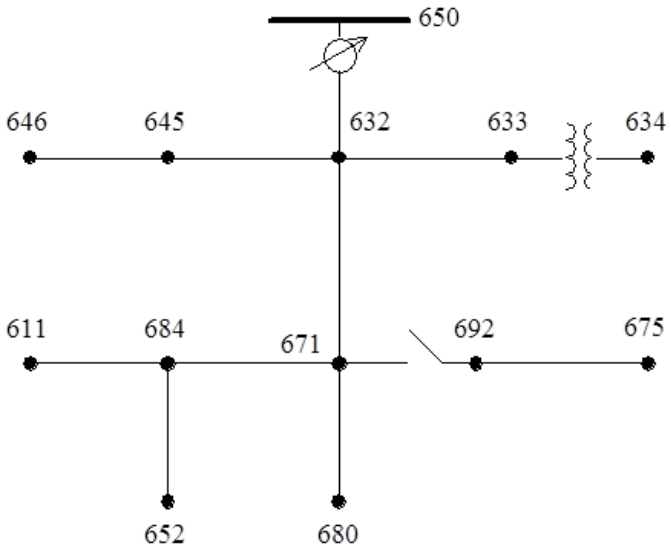


**Figure 1.** IEEE 13-node test feeder

In order to adequately assess the transient overvoltage transfer, the high-frequency model of the network's constituents was included. As an example, the capacitive coupling model between transformer windings had a value of 5 pF. On the other hand, to assess flashover in the network due to dielectric stress, the insulation coordination model in the medium voltage structures considered the basic insulation level (BIL) and the critical flashover (CFO). For the specific case of the selected region of Colombia, the BIL value included the altitude correction factor, considering an altitude of 2600 m above sea level. In addition, we included correction for environmental pollution, rated as moderate to high, and a grounding system, which considered an impedance at neutral bushing for the HV/MV transformers.

Therefore, the BIL values were 95-170 kV [36]. The surge arresters were only located in the transformers [5], [37]-[44].

Direct lightning strokes were distributed along sections 632-633, 671-680, and 632-671. Section 632-671 was divided into ten parts, with strokes covering 10, 50, and 90% of the network.

The point of registration for transient overvoltage resulting from direct lightning strokes was the transformer head, located between nodes 650 and 632 on the secondary side, with a voltage level of 13.2 kV.

### 2.2. Current pulse generator

Lightning has an 8/20 μs waveform, with peak currents of 3, 10, 20, 50, 80, and 100 kA. The direct strokes on the IEEE 13-node network occurred in phases A and C. Fig. 2 present the generated current waveform.

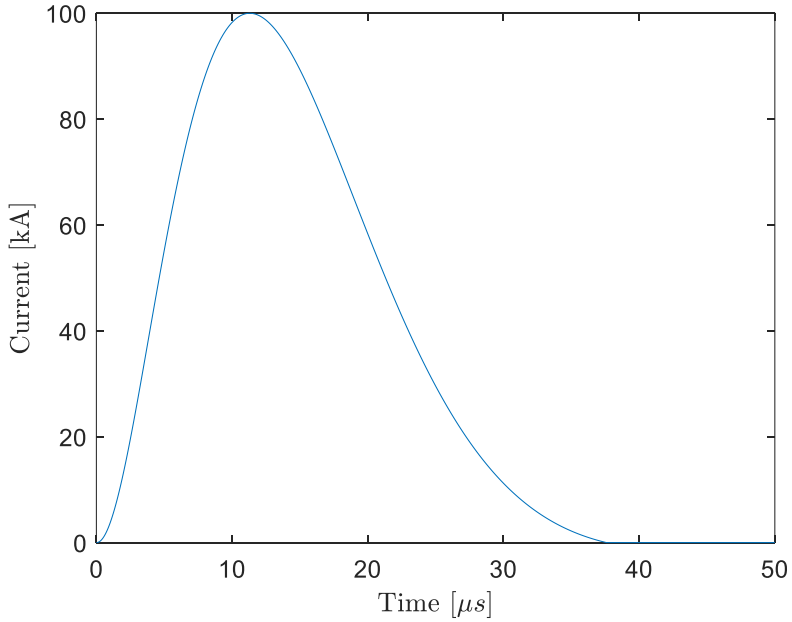


**Figure 2.** Current transient signal with an 8/20 μs waveform

The selection of the previously listed current magnitudes was based on the CIGRE and IEEE stroke current probability curves (Fig. 3), thereby ensuring that our study covered the spectrum of possible magnitudes in the analyzed geographic area [6], [45]-[47].

The IEEE 1410-2010 standard presents the statistical distribution of measurements obtained from towers, with a mean value of 31 kA [45], [48]. In IEEE 998-2012, the mean value ranges from 24 to 31 kA, and, in IEEE 1243-1997, the normalized mean value is 31 kA. This value is 31.1 kA in CIGRE 63 [49]-[51].

Throughout the Colombian territory, the distribution of positive and negative discharges is 31 and 69% with respect to the total lightning strokes [36]. It is noteworthy that 50% of the cloud-to-ground lightning equals or exceeds the value of 35 kA.

https://doi.org/10.14483/23448393.23305

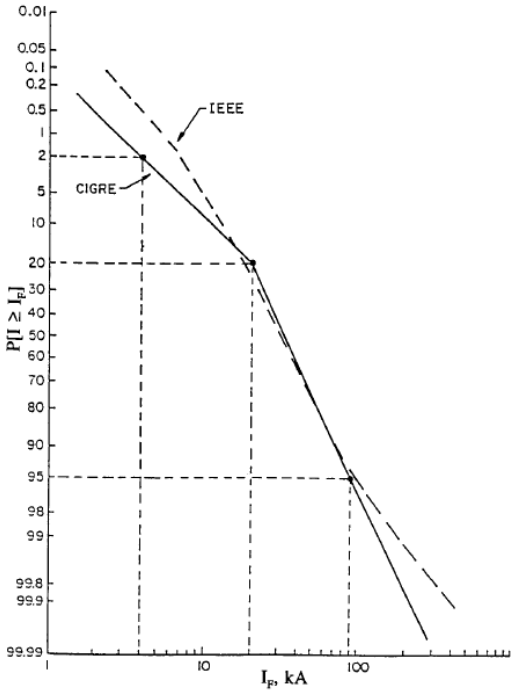


**Figure 3.** CIGRE and IEEE stroke current probability curves, first stroke Negative downward flash [4].

## 3. GoogLeNet, Python, and ChatGPT

The GoogLeNet deep learning neural network was implemented in MATLAB's Deep Network Designer, with a depth of 22, a size of 27 MB, seven million parameters, and an image input size of 224 x 224 pixels. The dataset used in this research contained RGB-type images, so we had to condition them to a size of 224 x 224 x 3 as an input parameter for the network. Fig. 4 depicts the architecture of the neural network.

**Figure 4.** GoogLeNet neural network architecture in MATLAB

The final blocks of GoogLeNet were adapted, ensuring a correct response to the number of classes entered. The ClassOutput layer (*i.e.*, the last one) and the FullyConnected layer were replaced to support five classes. Fig. 5 shows the replaced layers.

https://doi.org/10.14483/23448393.23305

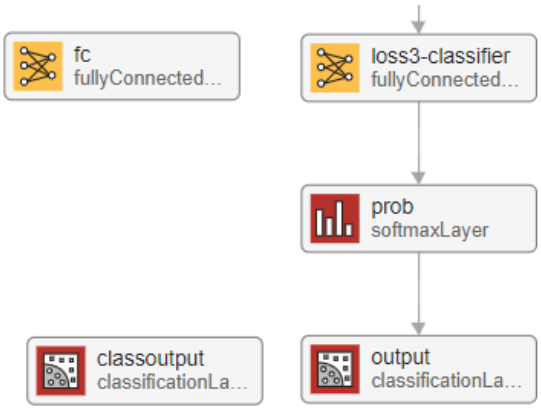


**Figure 5.** Replaced GoogLeNet layers

Table I presents the pseudocode for our neural network, which was developed in collaboration with ChatGPT [52]. The optimal hyperparameters are as follows: filters_1: 64, kernel_size_1: 4, conv_layers: 3, filters_2: 96, kernel_size_2: 5, units: 320, learning_rate: 0.001, filters_3: 32, kernel_size_3: 3, filters_4: 80, kernel_size_4: 3.

**Table I**

**Pseudocode for the Python neural network developed in collaboration with ChatGPT**

***Input: Image dataset distributed into five classes.***
**Output: trained and validated neural network for image classification**
|1| **Mount Google Drive**|
|2| Import necessary libraries: pandas, tensorflow, sklearn.model_selection|
|3| Define dataset_path|
|4| Define function create_dataframe_from_images(dataset_path) |
|5| Call create_dataframe_from_images(dataset_path) and assign it to image_df|
|6| Print image_df.head()|
|7| Import matplotlib.pyplot and cv2|
|8| Define function visualize_dataset_per_class(df, num_samples)|
|9| Call visualize_dataset_per_class(image_df, num_samples=5)|
|10| Define datagen|
|11| Define train_generator|
|12| Define validation_generator|
|13| Import keras, layers, kerastuner|
|14| Define function model_builder(hp) |
|15| Define tuner|
|16| Define class ClearTrainingOutput(tf.keras.callbacks.Callback)|
|17| Execute tuner.search() with specified arguments and callbacks|
|18| Get the best hyperparameters with tuner.get_best_hyperparameters(num_trials=1)[0]|
| 19| Print best hyperparameters|
|20| Import EarlyStopping and define early_stopping|
|21| Build model with tuner.hypermodel.build(best_hps)|
|22| Train the model with the specified parameters and callbacks|

https://doi.org/10.14483/23448393.23305

## 4. Methodology

Initially, the IEEE 13-node feeder was modeled in the EMTP-ATP software, in order to record the transient overvoltage from direct lightning strokes at the head of the network. Subsequently, the records were converted from the time domain to the frequency domain using the MATLAB software.

Once the five dataset classes with transient signals in the frequency domain had been constructed, the neural networks were performed in MATLAB and Python-ChatGPT. Fig. 6 presents the transformation of the transient signal. The transient signal in the time domain has no scaling regarding the overvoltage magnitude. Fig. 6 shows the records of direct lightning stroke, measured at the head of the feeder (20 kA at L632-671, 10% distance from L632 node).

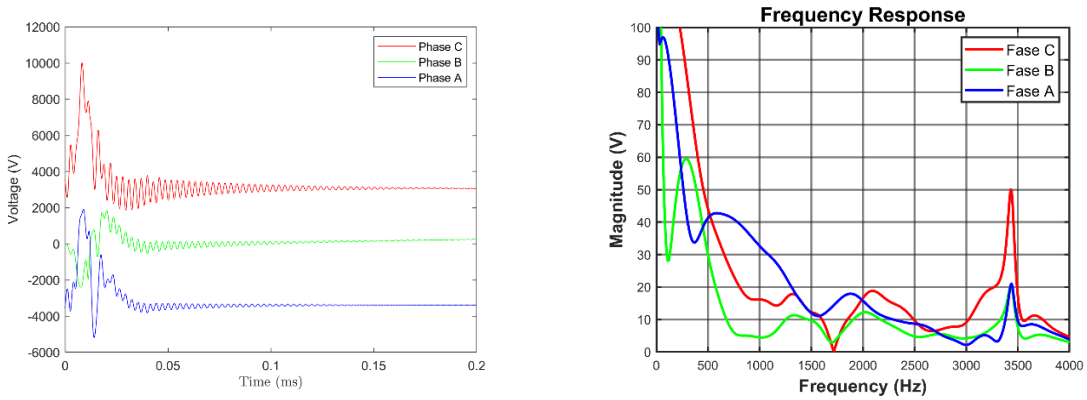


**Figure 6.** Transient signals in the time and frequency domains

## 5. Analysis of the results

The dataset was composed of 60 records of transient overvoltage in the frequency domain. As an example, Fig. 7 shows the frequency response of nine records with return stroke currents of 3, 50, and 100 kA and a waveform of 8/20 μs in phase C. The impact points with records of 13.2 kV at the feeder head are L632-633, L632-671 (50% distance from L632 node), and L671-680.

The format of the transient overvoltage records was PNG (Portable Network Graphics) format. The distribution of the dataset was 70% for training and 30% for testing in GoogLeNet. As for Python-ChatGPT, the distribution was 80% for training and 20% for testing.

Fig. 7 shows that, as the distance from the lightning stroke to the measurement point increases, frequencies above 1 kHz are attenuated. Therefore, the system behaves like a low-pass filter, which is consistent with the capacitive model of MV networks, the operation of surge arresters, and the electrical disruption of the insulator chain (pin insulator) of the poles supporting the MV overhead conductors, among other aspects.

On the other hand, frequencies below 1 kHz experience an increase in magnitude in some cases, given the reflection caused by changes in the characteristic impedance along the different branches of the MV system.

https://doi.org/10.14483/23448393.23305

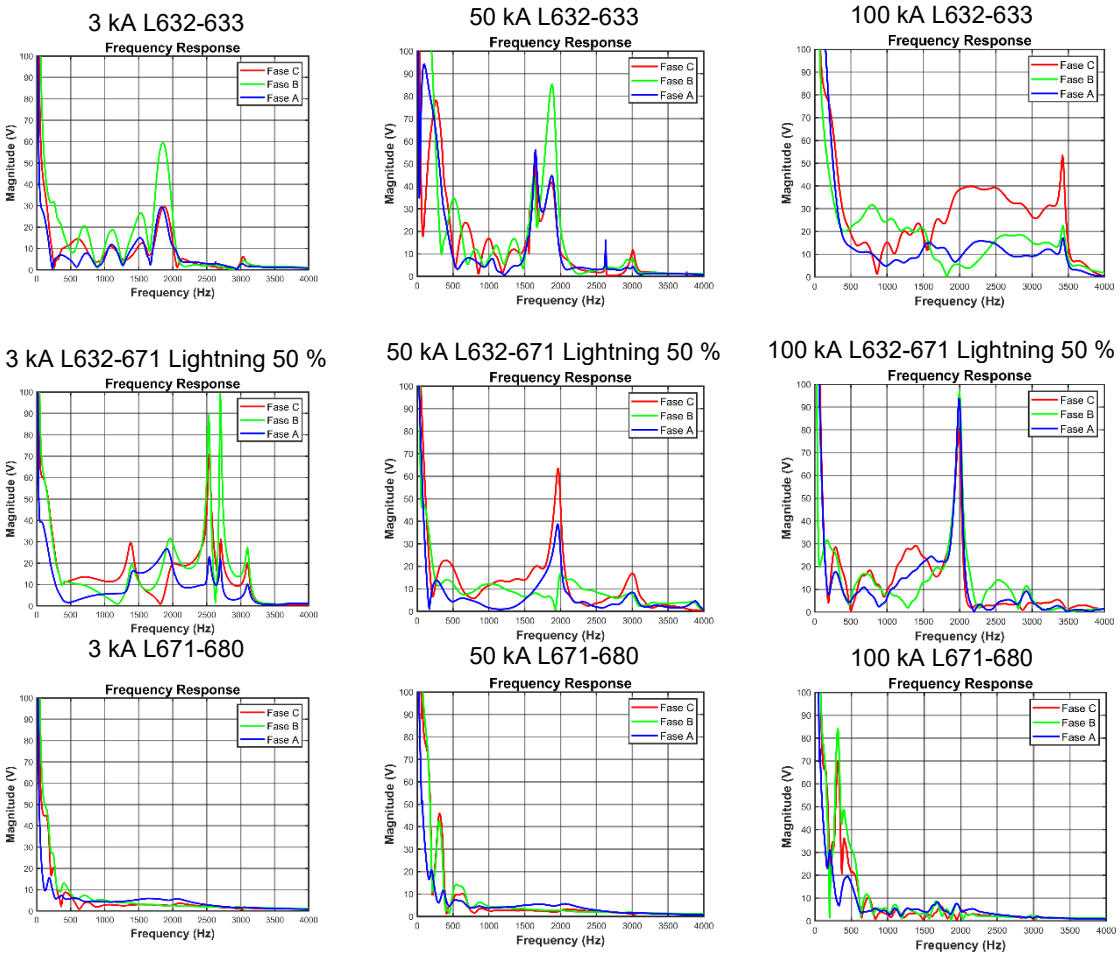


**Figure 7.** Frequency-domain transient overvoltage records from the feeder head

Table II presents the parameterization of each trained instance of GoogLeNet along with its accuracy. The best results were obtained by Network 3, with a value of 80%.

**Table II**

**Summary of the parameters used for our instances of the GoogLeNet deep learning network**

| Trained network | Validation frequency | *Max* epochs | *MiniBatch* size | Validation accuracy [%] |
|---|---|---|---|---|
| **E1** | 1 | 200 | 12 | **60** |
| **2** | 10 | 150 | 10 | **50** |
| **3** | 1 | 200 | 24 | **80** |
| **4** | 1 | 200 | 36 | **60** |
| **5** | **24** | **150** | **24** | **75** |

trainedNetwork_5 and trainedNetwork_6 reported accuracies of 85 and 45%, respectively. These are the pretrained neural networks with the best and worst results. The difference in their parameterization corresponds to the *MiniBatch* size: 12 for trainedNetwork_5 and 24

https://doi.org/10.14483/23448393.23305

for trainedNetwork_6. All neural networks were trained with the Adam solver, selecting the best evaluation point.

Four images from the dataset were evaluated to appropriately classify the frequency transient overvoltage measured at the 13.2 kV feeder head. The results of said classification show an adequate response when it comes to identifying direct lightning strokes with a peak value of 20 kA. Fig. 8 (1:1) shows a direct stroke in network segment L632-633. The (1:2) image reports a direct stroke in network segment L632-671, covering 90% of the line. The (2:1) image shows a direct stroke in network segment L632-671, covering 10% of the line, and the (2:2) image reports a direct stroke in network segment L671-680.

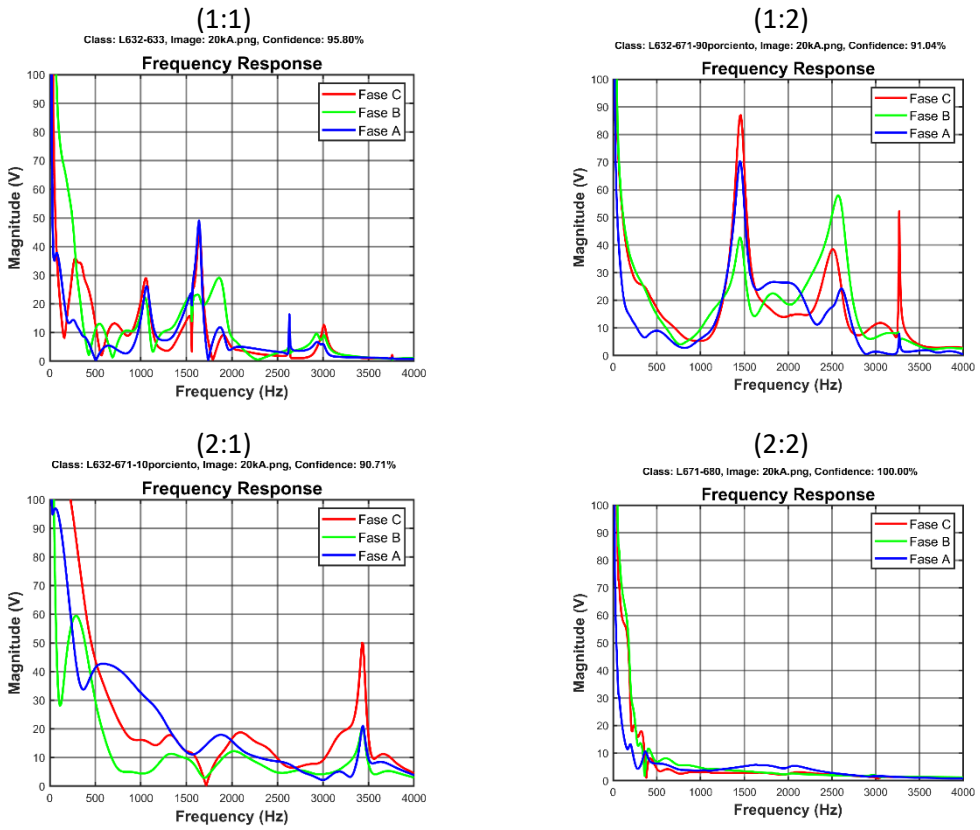


**Figure 8.** Image classification of the dataset

Fig. 9 presents the CDF and PDF of the confidence analysis for each of the segments containing the frequency response images. It should be highlighted that segments L671-680 and L632-671 exhibit the highest confidence during image classification, with values above 90%. Sections L632-671 (10%) and L632-633 (50%), with similar characteristic impedances for MV networks, tend to compromise confidence. However, a confidence percentage above 70% can be estimated for L632-633, L632-671 (10 and 90%), and L761-680 when classifying the frequency response.

https://doi.org/10.14483/23448393.23305

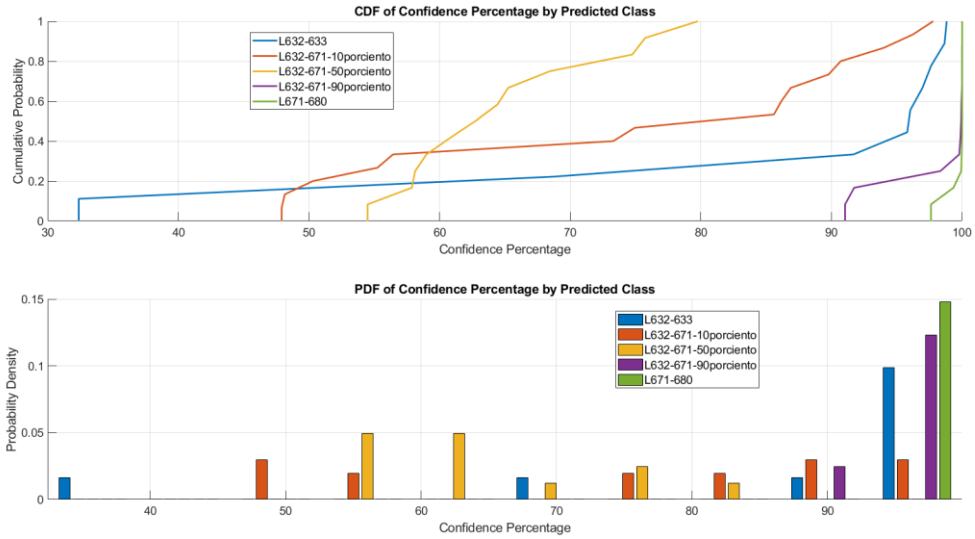


**Figure 9.** CDF and PDF of the confidence analysis of the segments

Proper modeling of a MV network, which includes the PI model of the network and the surge arresters, the capacitive impedances of transformers, the frequency response of the grounding system, the capacitive model of the underground cables (*e.g.*, section L692-675), and the tuning (or not) of the characteristic impedances, allows filtering multiples of the system's fundamental component. For example, the PI model of the transmission line behaves as a second-order filter for signal filtering. Therefore, at impact points far from the head of the MV circuit, where the transient overvoltage is recorded, it exhibits a better response for the classification of frequency response images.

When evaluating the confidence results for sections L632-671 and L632-633, considering the impact of a 20 kA atmospheric electrical discharge on phases A and C, note that the classification is compromised since they have very similar reflection coefficients, which is caused by changes in characteristic impedance.

Figs. 10 and 11 present the evolution of the loss and accuracy variables for each epoch for the neural network developed using with ChatGPT, which was implemented in the Google Colab Python environment. The maximum overfitting values for accuracy and loss are 0.3237 at epoch 6 and 0.3585 at epoch 35. The average overfitting values are 0.1269 and 0.1128, respectively.

From a maintenance, construction, and design engineering perspective, identifying the lightning impact point would enable a faster restoration of the power supply and positively impact service quality indicators such as the SAIDI/SAIFI [53]. Some studies have shown that the impacts of atmospheric electrical discharges on the shield wires of the transmission lines can deteriorate optical ground wires (OPGWs) (on average, 36 pairs of fiber optic cables) [54], [55], which enable communication for various substation services (*e.g.*, channel 85 for line differentials; the acceleration of tripping zones in the backup functions 21/21N in POTT schemes, which have a zone 2 comparison; and 67N, with directional comparison; among others) [56], [57]. This type of communication is structured using single-mode fiber optic, and some fibers that are not active—also known as *dark fibers*—are arranged in pair organizers in the substation [56]-[72].

https://doi.org/10.14483/23448393.23305

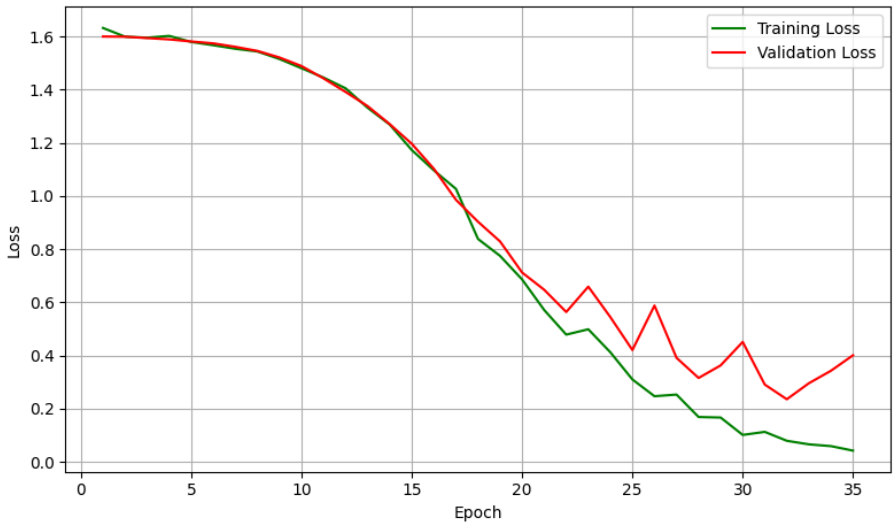


**Figure 10.** Evolution of the loss variable with respect to each epoch

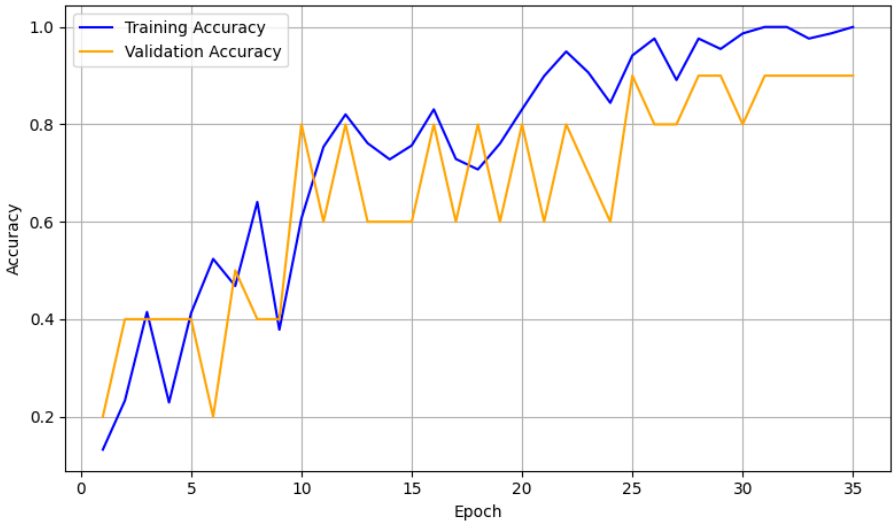


**Figure 11.** Evolution of the accuracy variable with respect to each epoch

Some illuminated fiber optic pairs are used for communication between the substation and the telecontrol (SCADA) center. The information transmitted through these channels is structured in frames following the IEC 60870-5-104 standard, which is supported by TCP/IP addressing. Before leaving the substation, the structured frame is formed in the gateway, which functions as a translator from the IEC 61850/DNP3 (distributed network protocol) standard to IEC 60870-5-104 [73]-[76]. Subsequently, it is routed through the substation firewall-router via multimode fiber. Finally, it is arranged in the optical distribution frame's (ODF) fiber optic pair before exiting the substation through the transmission line [67]-[70].

Failures in the illuminated fiber optic pairs require lighting dark fibers, thus reducing the availability of single-mode optical fibers. For example, in some communication architectures, it is possible to use equipment for data transmission serialization/multiplexing. This helps to reduce the physical occupation of communication channels [78]-[81]. On the other hand, the characterization of transient overvoltage resulting from direct lightning strokes allows

https://doi.org/10.14483/23448393.23305

designing adequate electrical infrastructure to favor operation and ensure safety and health conditions for network operators.

## 6. Mathematical contribution to electromagnetic coupling

The authors propose two physical-mathematical contributions in the frequency domain. The first one enhances the complex expression for permittivity and permeability, with applications in transverse electromagnetic (TEM) fields with arbitrary propagation, which was initially introduced in [84]. The second contribution applies complex permittivity and permeability expressions to the coupling of lightning on transmission lines.

Initially, the authors stated [84] that all media incur losses, both conductive and dielectric-polarization losses. Therefore, for linear isotropic media, constitutive relations are given by the following differential equations for the fields $\overline{E}$ and $\overline{H}$:

$$\overline{\boldsymbol{D}} = \boldsymbol{\varepsilon}\overline{\boldsymbol{E}} + \boldsymbol{\varepsilon_1}\frac{\partial\overline{\boldsymbol{E}}}{\partial \boldsymbol{t}} + \boldsymbol{\varepsilon_2}\frac{\partial^2\overline{\boldsymbol{E}}}{\partial \boldsymbol{t}^2} + \cdots \tag{1}$$

$$\overline{\boldsymbol{B}} = \boldsymbol{\mu}\overline{\boldsymbol{H}} + \boldsymbol{\mu_1}\frac{\partial\overline{\boldsymbol{H}}}{\partial \boldsymbol{t}} + \boldsymbol{\mu_2}\frac{\partial^2\overline{\boldsymbol{H}}}{\partial \boldsymbol{t}^2} + \cdots \tag{2}$$

Eqs. (1) and (2) can be expressed as presented below:

$$\overline{\boldsymbol{D}} = \boldsymbol{\varepsilon}\overline{\boldsymbol{E}} + \boldsymbol{jw\varepsilon_1}\,\overline{\boldsymbol{E}} - \boldsymbol{w^2\varepsilon_2}\,\overline{\boldsymbol{E}} - \boldsymbol{jw^3\varepsilon_3}\,\overline{\boldsymbol{E}} + \cdots \tag{3}$$

$$\overline{\boldsymbol{B}} = \boldsymbol{\varepsilon}\overline{\boldsymbol{H}} + \boldsymbol{jw\mu_1}\,\overline{\boldsymbol{H}} - \boldsymbol{w^2\mu_2}\,\overline{\boldsymbol{H}} - \boldsymbol{jw^3\mu_3}\,\overline{\boldsymbol{H}} + \cdots \tag{4}$$

The complex permittivity $\dot{\varepsilon_{(w)}}$ and the complex permeability $\dot{\mu_{(w)}}$ are defined as follows:

$$\dot{\boldsymbol{\varepsilon}_{(\boldsymbol{w})}} = \boldsymbol{\varepsilon}'(\boldsymbol{w}) - \boldsymbol{j}\boldsymbol{\varepsilon}''(\boldsymbol{w}) \tag{5}$$

$$\dot{\boldsymbol{\mu}_{(\boldsymbol{w})}} = \boldsymbol{\mu}'(\boldsymbol{w}) - \boldsymbol{j}\boldsymbol{\mu}''(\boldsymbol{w}) \tag{6}$$

Thus, the constitutive relations take the following complex form:

$$\overline{\boldsymbol{D}} = \dot{\boldsymbol{\varepsilon}_{(\boldsymbol{w})}}\,\overline{\boldsymbol{E}} = \boldsymbol{\varepsilon}'_{(\boldsymbol{w})}\,\overline{\boldsymbol{E}} - \boldsymbol{j}\boldsymbol{\varepsilon}''_{(\boldsymbol{w})}\,\overline{\boldsymbol{E}} \tag{7}$$

$$\overline{\boldsymbol{B}} = \dot{\boldsymbol{\mu}_{(\boldsymbol{w})}}\,\overline{\boldsymbol{H}} = \boldsymbol{\mu}'_{(\boldsymbol{w})}\,\overline{\boldsymbol{H}} - \boldsymbol{j}\boldsymbol{\mu}''_{(\boldsymbol{w})}\,\overline{\boldsymbol{H}} \tag{8}$$

Maxwell's equations in complex form are as follows:

$$\overline{\boldsymbol{\nabla}}\boldsymbol{x}\overline{\boldsymbol{E}} = -\boldsymbol{jw}\dot{\boldsymbol{\mu}_{(\boldsymbol{w})}}\,\overline{\boldsymbol{H}} = -\boldsymbol{jw}\boldsymbol{\mu}'_{(\boldsymbol{w})}\,\overline{\boldsymbol{H}} - \boldsymbol{w}\boldsymbol{\mu}''_{(\boldsymbol{w})}\,\overline{\boldsymbol{H}} \tag{9}$$

https://doi.org/10.14483/23448393.23305

$$\overline{\nabla} x \overline{H} = jw\dot{\varepsilon_{(w)}}\,\overline{E} + \sigma\overline{E} + \overline{J} = jw\varepsilon'_{(w)}\,\overline{E} + w\varepsilon''_{(w)}\,\overline{E} + \sigma\overline{E} + \overline{J} \tag{10}$$

$$\overline{\nabla} \cdot \dot{\varepsilon_{(w)}}\overline{E} = \overline{\nabla} \cdot \left(\varepsilon'_{(w)} - j\varepsilon''_{(w)}\right)\overline{E} = \rho \tag{11}$$

$$\overline{\nabla} \cdot \dot{\mu_{(w)}}\overline{H} = \overline{\nabla} \cdot \left(\mu'_{(w)} - j\mu''_{(w)}\right)\overline{H} = 0 \tag{12}$$

For a conductive medium, $\sigma$ and $w\varepsilon''_{(w)}$ are factors of the same type. Eq. 10 can be rewritten in the same way:

$$\overline{\nabla} x \overline{H} = jw\dot{\varepsilon_{(w)}}\,\overline{E} + \sigma\overline{E} + \overline{J} = jw\varepsilon'_{(w)}\,\overline{E} + w\varepsilon''_{(w)}\,\overline{E} + \sigma\overline{E} + \overline{J} \tag{13}$$

$$\overline{\nabla} x \overline{H} = jw\varepsilon'_{(w)}\,\overline{E} + jw\left(-j\varepsilon''_{(w)} - j\frac{\sigma}{w}\right)\overline{E} + \overline{J} \tag{14}$$

$$\overline{\nabla} x \overline{H} = jw\left(\varepsilon'_{(w)} - j\varepsilon''_{(w)} - j\frac{\sigma}{w}\right)\overline{E} + \overline{J} \tag{15}$$

where

$$\dot{\varepsilon_{(w)}} = \varepsilon'_{(w)} - j\left(\varepsilon''_{(w)} + \frac{\sigma}{w}\right) \tag{16}$$

The loss tangent is

$$tan\delta = \frac{w\varepsilon'' + \sigma}{w\varepsilon'} \tag{17}$$

In a lossy medium, the complex wave equations (Helmholtz equations) are

$$\overline{\nabla}^2\,\overline{E} + w^2\dot{\mu_{(w)}}\left[\varepsilon'_{(w)} - j\left(\varepsilon''_{(w)} + \frac{\sigma}{w}\right)\right]\overline{E} = 0 \tag{18}$$

$$\overline{\nabla}^2\,\overline{H} + w^2\dot{\mu_{(w)}}\left[\varepsilon'_{(w)} - j\left(\varepsilon''_{(w)} + \frac{\sigma}{w}\right)\right]\overline{H} = 0 \tag{19}$$

From this point onward, the authors will decompose the complex permeability expression in order to explicitly identify the phase and attenuation coefficients, as shown in Eqs. (20)-(23):

$$|\overline{k}| = w\sqrt{\dot{\mu_{(w)}}\,\dot{\varepsilon_{(w)}}} \tag{20}$$

$$|\overline{k}| = w\sqrt{\dot{\mu_{(w)}}\,\dot{\varepsilon_{(w)}}} = w\sqrt{\dot{\mu_{(w)}}\,\left(\varepsilon'_{(w)} - j\left(\varepsilon''_{(w)} + \frac{\sigma}{w}\right)\right)} \tag{21}$$

https://doi.org/10.14483/23448393.23305

$$|\overline{k}| = w\sqrt{(\mu'_{(w)} - j\mu''_{(w)})\left(\varepsilon'_{(w)} - j\left(\varepsilon''_{(w)} + \frac{\sigma}{w}\right)\right)} \tag{22}$$

$$|\overline{k}| = w\sqrt{\left(\mu'_{(w)}\varepsilon'_{(w)} - j\mu'_{(w)}\left(\varepsilon''_{(w)} + \frac{\sigma}{w}\right) - j\mu''_{(w)}\varepsilon'_{(w)} - \mu''_{(w)}\left(\varepsilon''_{(w)} + \frac{\sigma}{w}\right)\right)} \tag{23}$$

As

$$\overline{\gamma} = j|\overline{k}| = \alpha + j\beta \tag{24}$$

$$|\overline{k}| = \beta - j\alpha \tag{25}$$

Where each expression corresponds to the propagation coefficient $\overline{\gamma}$, the attenuation coefficient $\alpha$ , and the phase coefficient $\beta$. This is shown in Eqs. (26)-(35).

$$|\overline{k}|^2 = (\beta - j\alpha)^2 = \beta^2 - j\alpha\beta - j\alpha\beta - \alpha^2 \tag{26}$$

$$|\overline{k}|^2 = (\beta^2 - \alpha^2) - 2j\alpha\beta \tag{27}$$

$$|\overline{k}|^2 = w^2\left[\mu'_{(w)}\varepsilon'_{(w)} - \mu''_{(w)}\left(\varepsilon''_{(w)} + \frac{\sigma}{w}\right)\right] - jw^2\left[\mu'_{(w)}\left(\varepsilon''_{(w)} + \frac{\sigma}{w}\right) + \mu''_{(w)}\varepsilon'_{(w)}\right] \tag{28}$$

$$(\beta^2 - \alpha^2) = w^2\left[\mu'_{(w)}\varepsilon'_{(w)} - \mu''_{(w)}\left(\varepsilon''_{(w)} + \frac{\sigma}{w}\right)\right] \tag{29}$$

$$2\alpha\beta = w^2\left[\mu'_{(w)}\left(\varepsilon''_{(w)} + \frac{\sigma}{w}\right) + \mu''_{(w)}\,\varepsilon'_{(w)}\right] \tag{30}$$

$$\left||\overline{k}|^2\right| = \sqrt{w^4\left[\left[\mu'_{(w)}\,\varepsilon'_{(w)} - \mu''_{(w)}\left(\varepsilon''_{(w)} + \frac{\sigma}{w}\right)\right]^2 + \left[\mu'_{(w)}\left(\varepsilon''_{(w)} + \frac{\sigma}{w}\right) + \mu''_{(w)}\,\varepsilon'_{(w)}\right]^2\right]} \tag{31}$$

$$\left||\overline{k}|^2\right| = w^2\left[\mu'_{(w)}\,\varepsilon'_{(w)} - \mu''_{(w)}\left(\varepsilon''_{(w)} + \frac{\sigma}{w}\right)\right]\sqrt{\left[1 + \frac{\left[\mu'_{(w)}\left(\varepsilon''_{(w)} + \frac{\sigma}{w}\right) + \mu''_{(w)}\,\varepsilon'_{(w)}\right]^2}{\left[\mu'_{(w)}\,\varepsilon'_{(w)} - \mu''_{(w)}\left(\varepsilon''_{(w)} + \frac{\sigma}{w}\right)\right]^2}\right]} \tag{32}$$

$$\left||\overline{k}|^2\right| = \sqrt{(\beta^2 - \alpha^2)^2 + (2\alpha\beta)^2} = \sqrt{\beta^4 - 2\beta^2\alpha^2 + \alpha^4 + (2\alpha\beta)^2} \tag{33}$$

$$\left||\overline{k}|^2\right| = \sqrt{(\beta^4 + \alpha^4) + (2\alpha^2\beta^2)} = \sqrt{(\alpha^2 + \beta^2)^2} = \alpha^2 + \beta^2 \tag{34}$$

$$Re\left(|\overline{k}|^2\right) = \beta^2 - \alpha^2 = w^2\left[\mu'_{(w)}\,\varepsilon'_{(w)} - \mu''_{(w)}\left(\varepsilon''_{(w)} + \frac{\sigma}{w}\right)\right] \tag{35}$$

Therefore,

$$\left|\overline{|k|}\right| + Re\left(|\overline{k}|^2\right) = 2\beta^2 = w^2\left[\mu'_{(w)}\,\varepsilon'_{(w)} - \mu''_{(w)}\left(\varepsilon''_{(w)} + \frac{\sigma}{w}\right)\right]\cdot\left[1 + \sqrt{1 + \frac{\left[\mu'_{(w)}\left(\varepsilon''_{(w)} + \frac{\sigma}{w}\right) + \mu''_{(w)}\,\varepsilon'_{(w)}\right]^2}{\left[\mu'_{(w)}\,\varepsilon'_{(w)} - \mu''_{(w)}\left(\varepsilon''_{(w)} + \frac{\sigma}{w}\right)\right]^2}}\right] \tag{36}$$

The phase coefficient is determined by Eq. (37):

https://doi.org/10.14483/23448393.23305

$$\boldsymbol{\beta} = \frac{w}{\sqrt{2}}\sqrt{\left[\boldsymbol{\mu}'_{(w)}\,\boldsymbol{\varepsilon}'_{(w)} - \boldsymbol{\mu}''_{(w)}\left(\boldsymbol{\varepsilon}''_{(w)} + \frac{\sigma}{w}\right)\right]} \cdot \sqrt{\left[1 + \sqrt{1 + \frac{\left[\mu'_{(w)}\left(\varepsilon''_{(w)} + \frac{\sigma}{w}\right) + \mu''_{(w)}\,\varepsilon'_{(w)}\right]^2}{\left[\mu'_{(w)}\,\varepsilon'_{(w)} - \mu''_{(w)}\left(\varepsilon''_{(w)} + \frac{\sigma}{w}\right)\right]^2}}\right]} \tag{37}$$

In addition,

$$\left|\left|\overline{k}\right|^2\right| - Re\left(\left|\overline{k}\right|^2\right) = (\alpha^2 + \beta^2) - (\beta^2 - \alpha^2) = 2\alpha^2 \tag{38}$$

$$2\alpha^2 = w^2\left[\boldsymbol{\mu}'_{(w)}\,\boldsymbol{\varepsilon}'_{(w)} - \boldsymbol{\mu}''_{(w)}\left(\boldsymbol{\varepsilon}''_{(w)} + \frac{\sigma}{w}\right)\right] \cdot \sqrt{1 + \frac{\left[\mu'_{(w)}\left(\varepsilon''_{(w)} + \frac{\sigma}{w}\right) + \mu''_{(w)}\varepsilon'_{(w)}\right]^2}{\left[\mu'_{(w)}\varepsilon'_{(w)} - \mu'_{(w)}\left(\varepsilon''_{(w)} + \frac{\sigma}{w}\right)\right]^2}} - w^2\left[\boldsymbol{\mu}'_{(w)}\,\boldsymbol{\varepsilon}'_{(w)} - \boldsymbol{\mu}''_{(w)}\left(\boldsymbol{\varepsilon}''_{(w)} + \frac{\sigma}{w}\right)\right] \tag{39}$$

The attenuation coefficient is determined by Eq. (40):

$$\boldsymbol{\alpha} = \frac{w}{\sqrt{2}}\sqrt{\left[\boldsymbol{\mu}'_{(w)}\,\boldsymbol{\varepsilon}'_{(w)} - \boldsymbol{\mu}''_{(w)}\left(\boldsymbol{\varepsilon}''_{(w)} + \frac{\sigma}{w}\right)\right]} \cdot \sqrt{\sqrt{1 + \frac{\left[\mu'_{(w)}\left(\varepsilon''_{(w)} + \frac{\sigma}{w}\right) + \mu''_{(w)}\varepsilon'_{(w)}\right]^2}{\left[\mu'_{(w)}\varepsilon'_{(w)} - \mu'_{(w)}\left(\varepsilon''_{(w)} + \frac{\sigma}{w}\right)\right]^2}} - 1} \tag{40}$$

In a lossy medium, the wave impedance also becomes complex, as shown in Eq. (41).

$$\dot{\eta} = \sqrt{\frac{\mu'_{(w)} - j\,\mu''_{(w)}}{\varepsilon'_{(w)} - j\left(\varepsilon'' + \frac{\sigma}{w}\right)}} \tag{41}$$

The authors propose implementing complex-valued expressions for permittivity and permeability within the lightning-coupling model (Fig. 12).

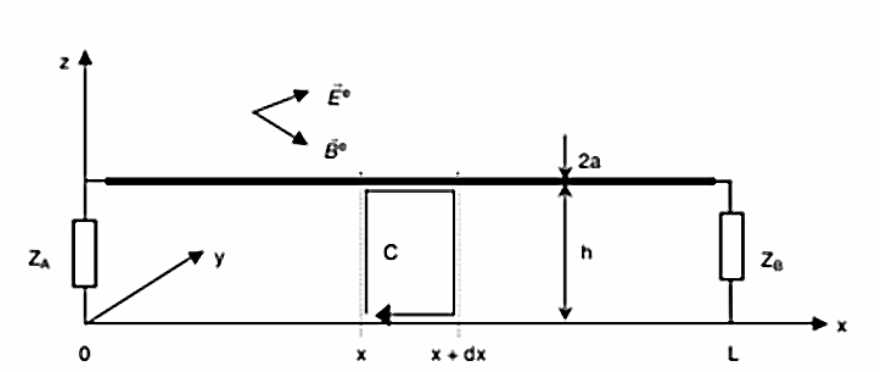


**Figure 12.** Lightning-coupling model [85]

As presented in the previous sections in both integral and differential forms, as shown in Eqs. (42) and (43).

https://doi.org/10.14483/23448393.23305

$$\overline{\nabla} x \overline{E} = -jw\dot{\mu}_{(w)}\,\overline{H} = -jw\mu'_{(w)}\,\overline{H} - jw\mu''_{(w)}\,\overline{H} = -jw\overline{B} \quad (42)$$

$$\oint \overline{E}\cdot dl = -\int jw\dot{\mu}_{(w)\overline{H}}\cdot d\overline{s} = -\int jw\overline{B}\cdot d\overline{s} \quad (43)$$

The above is determined for contour CCC (differential form with Ax):

$$\int_0^h \overline{E}_{(x,z)}\cdot d\overline{z} + \int_x^{x+\Delta x} \overline{E}_{(x,h)}\cdot d\overline{x} + \int_h^0 \overline{E}_{(x+\Delta x,z)}\cdot d\overline{z} + \int_{x+\Delta x}^{x} \overline{E}_{(x,0)}\cdot d\overline{x} = -jw\int_0^h\int_x^{x+\Delta x}\overline{B}_{(x,z)}\cdot dxdz\overline{ay} \quad (44)$$

$$\int_0^h \overline{E}_{(x,z)}\cdot d\overline{z} - \int_0^h \overline{E}_{(x+\Delta x,z)}\cdot d\overline{z} + \int_x^{x+\Delta x} \overline{E}_{(x,h)}\cdot d\overline{x} - \int_x^{x+\Delta x} \overline{E}_{(x,0)}\cdot d\overline{x} = -jw\int_0^h\int_x^{x+\Delta x}\overline{B}_{(x,z)}\cdot dxdz\overline{ay} \quad (45)$$

$$-\int_0^h \left[\left|\overline{E}_{z(x+\Delta x,z)}\right| - \left|\overline{E}_{z(x,z)}\right|\right]dz + \int_x^{x+\Delta x}\left[\left|\overline{E}_{x(x,h)}\right| - \left|\overline{E}_{x(x,0)}\right|\right]dx = -jw\int_0^h\int_x^{x+\Delta x}\left|\overline{B}_{y(x,z)}\right|dxdz \quad (46)$$

Taking the partial derivative with respect to x on both sides of the equation yields the following expression:

$$-\frac{\partial}{\partial x}\int_0^h\left[\left|\overline{E}_{z(x+\Delta x,z)}\right| - \left|\overline{E}_{z(x,z)}\right|\right]dz = -jw\int_0^h\left|\overline{B}_{y(x,z)}\right|dz \quad (47)$$

On the other hand, from Faraday's law (quasi-static fields), it is possible to obtain Eq. (48):

$$V(x) = -\int \overline{E}\cdot d\overline{l} = -\int_0^h\left[\left|\overline{E}_{z(x+\Delta x,z)}\right| - \left|\overline{E}_{z(x,z)}\right|\right]dz \quad (48)$$

And then Eqs. (49) and (50):

$$\frac{\partial}{\partial x}[V(x)] = -jw\int_0^h\left|\overline{B}_{y(x,z)}\right|dz \quad (49)$$

$$\frac{\partial}{\partial x}[V(x)] = -jw\int_0^h\left|\overline{B}^{e}_{y(x,z)}\right|dz - jw\int_0^h\left|\overline{B}^{s}_{y(x,z)}\right|dz \quad (50)$$

From earlier derivations in both integral and differential form, it is possible to express the following:

https://doi.org/10.14483/23448393.23305

$$\overline{\nabla} x \overline{Hs} = \overline{Js} + jw\dot{\varepsilon}_{(w)} \overline{E} = jw\left(\varepsilon'_{(w)} - j\varepsilon''_{(w)} - j\frac{\sigma}{w}\right)\overline{E} + \overline{J} \quad (51)$$

$$\overline{\nabla} x \overline{Hs} = jw\overline{D} + \overline{J} \quad (52)$$

$$\int \overline{Hs} \cdot d\overline{l} = \int \overline{J} \cdot d\overline{s} + jw \int \overline{Ds} \cdot d\overline{s} \quad (53)$$

The inductance of the conductor can be determined using the following procedure:

$$\int \overline{H} \cdot d\overline{l} = \int \overline{J} \cdot d\overline{s} = Ience \quad (54)$$

$$\left|\overline{B_{\varphi}}\right| = \dot{\mu}_{(w)} \frac{Ience}{2\pi\rho} \quad (55)$$

$$\int \overline{B} \cdot d\overline{s} = L' \cdot Ience \int dz \quad (56)$$

The inductance per unit length can be expressed as presented below.

$$\int \left|\overline{B}\right| d\rho = L' \cdot Inece \quad (57)$$

Now, assuming the following expression:

$$\int \int \overline{B} \cdot d\overline{s} = \int \int \frac{\dot{\mu}_{(w)}}{2\pi\rho} Ience \cdot d\rho dz \quad (58)$$

If this is multiplied by $j\omega$, and we assume that $\omega$ does not vary with respect to $\rho$ and $z$, Eq. (59) is obtained.

$$jw \int \int \overline{B} \cdot d\overline{s} = jw \int \frac{\dot{\mu}_{(w)} Ience \cdot d\rho}{2\pi\rho} \int dz \quad (59)$$

The scattered field can be expressed as follows:

$$\int jw \int \left|\overline{B}\right| d\rho dz = \frac{jw\dot{\mu}_{(w)}}{2\pi\rho} Ience \ ln\frac{d2}{d1} \int dz = jwL \cdot Ience \int dz \quad (60)$$

Returning to Eqs. (49) and (50), this research implements the subscript s for the scattered field and the subscript e for the excitation field, in order to obtain the telegrapher's equation:

https://doi.org/10.14483/23448393.23305

$$\int_x^{x+x\Delta} \frac{\partial}{\partial x}[V(x)]dx = -jw \int_0^h \int_x^{x+\Delta x} \left|\overline{B}_{y(x,z)}\right| dxdz \tag{61}$$

$$\int_x^{x+x\Delta} \frac{\partial}{\partial x}[V(x)]dx = -\int_x^{x+\Delta x} jw \int_0^h \left|\overline{B}^s_{y(x,z)}\right| dzdx - \int_x^{x+\Delta x} jw \int_0^h \left|\overline{B}^e_{y(x,z)}\right| dzdx \tag{62}$$

$$\int_x^{x+x\Delta} \frac{\partial}{\partial x}[V(x)]dx = -\int_x^{x+\Delta x} jwL' I_{(x)} dx - \int_x^{x+\Delta x} jw \int_0^h \left|\overline{B}^e_{y(x,z)}\right| dzdx \tag{63}$$

$$\frac{\partial}{\partial x}[V(x)] + jwL' I_{(x)} = -jw \int_0^h \left|\overline{B}^e_{y(x,z)}\right| dz \tag{64}$$

On the other hand, Maxwell's equations can be expressed in pointwise (differential) form:

$$\overline{\nabla} x \overline{H} = \overline{J} + jw\dot{\varepsilon}_{(w)} \overline{E} \tag{65}$$

$$\overline{\nabla} x \overline{H} = \overline{J} + jw\overline{D} \tag{66}$$

$$\overline{\nabla} x \overline{H} = \left(\frac{\partial|\overline{H_z}|}{\partial y} - \frac{\partial|\overline{H_y}|}{\partial z}\right)\overline{ax} - \left(\frac{\partial|\overline{H_z}|}{\partial x} - \frac{\partial|\overline{H_x}|}{\partial z}\right)\overline{ay} + \left(\frac{\partial|\overline{H_y}|}{\partial x} - \frac{\partial|\overline{H_x}|}{\partial y}\right)\overline{az} \tag{67}$$

For the $z$-component,

$$\left(\frac{\partial|\overline{H_y}|}{\partial x} - \frac{\partial|\overline{H_x}|}{\partial y}\right)\overline{az} = \overline{J} + jw\dot{\varepsilon}_{(w)} \overline{E}_{(x,z)} \tag{68}$$

Since the medium is insulating, it follows that $\sigma_{isolation} = 0$. Therefore,

$$jw\overline{E}_{(x,z)} = \left(\frac{d|\overline{H}_y|}{dx} - \frac{d|\overline{H}_x|}{dy}\right) \cdot \frac{1}{\dot{\varepsilon}_{(w)}} \tag{69}$$

By integrating along the $z$-axis from 0 to $h$, we obtain the following for the scattered field and the excitation:

$$jw \int_0^h \left|\overline{E}_{(x,z)}\right| dz = -jwV(x) \tag{70}$$

$$jw \int_0^h \left|\overline{E}_{(x,z)}\right| dz = \frac{1}{\dot{\varepsilon}_{(w)}\,\dot{\mu}_{(w)}} \int_0^h \left[\frac{\partial \overline{B}^e_{y(x,z)}}{\partial x} - \frac{\partial \overline{B}^e_{x(x,z)}}{\partial y}\right] dz + \frac{1}{\dot{\varepsilon}_{(w)}\,\dot{\mu}_{(w)}} \int_0^h \left[\frac{\partial \overline{B}^s_{y(x,z)}}{\partial x} - \frac{\partial \overline{B}^s_{x(x,z)}}{\partial y}\right] dz \tag{71}$$

The excitation field and the scattered field are defined as follows:

https://doi.org/10.14483/23448393.23305

$$jw \int_0^h \left|\overline{E}^e_{(x,z)}\right| dz = \frac{1}{\dot{\varepsilon}_{(w)}\,\dot{\mu}_{(w)}} \int_0^h \left[\frac{\partial \overline{B}^e_{y(x,z)}}{\partial x} - \frac{\partial \overline{B}^e_{x(x,z)}}{\partial y}\right] dz \tag{72}$$

$$jw \int_0^h \left|\overline{E}^s_{(x,z)}\right| dz = \frac{1}{\dot{\varepsilon}_{(w)}\,\dot{\mu}_{(w)}} \int_0^h \left[\frac{\partial \overline{B}^s_{y(x,z)}}{\partial x} - \frac{\partial \overline{B}^s_{x(x,z)}}{\partial y}\right] dz \tag{73}$$

From the derivation for quasi-static fields, it is possible to obtain the following:

$$Q = \int \left|\overline{D}\right| \cdot d\overline{s} = \int \rho_v \, dv \tag{74}$$

$$\left|\overline{E}\right| = \frac{Q}{2\pi\rho\dot{\varepsilon}_{(w)} l} \tag{75}$$

$$C = \frac{Q}{V_{ab}} = \frac{\pi\dot{\varepsilon}_{(w)} l}{ln\frac{d}{r}} \tag{76}$$

Therefore,

$$V = -\int \overline{E} \cdot d\overline{l} = \frac{Q}{C} \tag{77}$$

$$C' V_{ab} = -C' \int \overline{E} \cdot d\overline{l} \tag{78}$$

$$jwC' V_{ab} = -jwC' \int \overline{E} \cdot d\overline{l} \tag{79}$$

Thus,

$$-jwV(x) = jw \int_0^h \left|\overline{E}^e_{(x,z)}\right| dz + jw \int_0^h \left|\overline{E}^s_{(x,z)}\right| dz| \tag{80}$$

$$-jwC'V(x) = jwC' \int_0^h \left|\overline{E}^e_{(x,z)}\right| dz + jwC' \int_0^h \left|\overline{E}^s_{(x,z)}\right| dz \tag{81}$$

$$-jwC' \int_0^h \left|\overline{E}^e_{(x,z)}\right| dz = jwC'V(x) + \frac{C'}{\dot{\varepsilon}_{(w)}\,\dot{\mu}_{(w)}} \int_0^h \left[\frac{\partial \overline{B}^s_{y(x,z)}}{\partial x}\right] dz \tag{82}$$

$\overline{B}^s_{x(x,z)} = 0$ since a TEM wave is present. Therefore,

$$-jwC' \int_0^h \left|\overline{E}^e_{(x,z)}\right| dz = jwC'V(x) + \frac{C'}{\dot{\varepsilon}_{(w)}\,\dot{\mu}_{(w)}} \frac{\partial[L' \cdot I]}{\partial x} \tag{83}$$

This can be expressed as follows, given that $L'C' = \varepsilon_{(\dot{w})}\ \mu_{(\dot{w})}$:

$$-\boldsymbol{jwC'}\ \int_0^h \left|\overline{\boldsymbol{E}}^{\boldsymbol{e}}_{(x,z)}\right| \boldsymbol{dz} = \boldsymbol{jwC'V(x)} + \frac{\partial[I]}{\partial x} \tag{84}$$

Below is the definition of the circuit with complex-field coupling. The original expression for electric and magnetic coupling can still be employed. However, it should be noted that permittivity and permeability are expressed in the complex domain and are frequency-dependent. Under the present notation, it is important to emphasize that the field $e$ is equal to the field $i$ in Fig. 13.

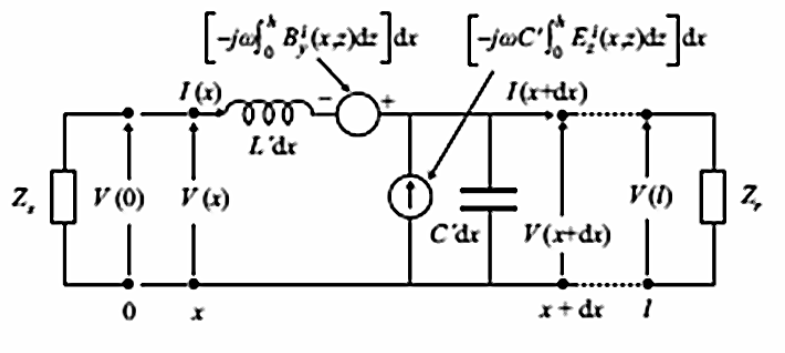


**Figure 13.** Equivalent circuit of TEM coupling [23]

## 7. Conclusions

Our implementation of neural networks based on GoogLeNet, Python, and ChatGPT for the classification of transient overvoltage resulting from direct lightning strokes in the frequency domain for branched radial networks showed an acceptable response, with accuracy values of 80 and 89.99%. The average overfitting of the network developed in collaboration with ChatGPT was 0.1269 for accuracy and 0.1128 for losses.

Furthermore, our review of 12 records of transient overvoltage due to lightning strokes on the L671-680 section shows close to 100% confidence in image classification using a pre-trained instance of GoogLeNet. The classification for the L632-633 section, under a direct lightning strike of 20 kA on phase A, reported a confidence of 32.38%, which was the worst result obtained.

The 60 frequency response images analyzed exhibited a confidence level above 70% for branches L632-633, L632-671 (10 and 90%), and L671-680.

The new mathematical formulation for the coupling of electromagnetic fields in polarized media improves upon the version proposed by Taylor (1965) [23], [85]. The authors considered the permeability and permittivity coefficients as complex quantities in order for the new coupling model to be applied to materials such as dielectrics (dry air, gas-insulated switchgear, arc chambers), ferroelectrics, and magnetic media (ferrites, cores, shielding), among others.

## 8. Author contributions

**Luis Eduardo Perdomo Orjuela**: conceptualization, data curation, formal analysis, investigation, validation, visualization, writing

**Francisco Santamaria Piedrahita**: conceptualization, data curation, formal analysis, investigation, supervision, validation, writing

**Nelson Enrique Vera Parra**: conceptualization, data curation, formal analysis, investigation, supervision, validation, writing

## 9. Acknowledgements

The authors would like to thank the members of the GISE3 and EMC-UN groups, attached to Universidad Distrital Francisco José de Caldas and Universidad Nacional de Colombia, respectively, for the support provided during this research.

## 10. Conflict of interest

The authors declare that they have no known competing financial interests or personal relationships that could appear to have influenced the study reported in this paper.

## 11. Use of artificial intelligence

During this work, the authors did not employ any technologies associated with artificial intelligence.

## References

[1] V. Cooray, *The Lightning Flash*. London, U.K.: Institution of Engineering and Technology, 2014. https://doi.org/10.1049/PBPO069E

[2] V. Cooray, *An Introduction to Lightning*. New York, NY, USA: Springer, 2016. https://doi.org/10.1007/978-94-017-8938-7

[3] V. Cooray, *Lightning Protection*. London, U.K.: Institution of Engineering and Technology, 2010. https://doi.org/10.1049/PBPO058E

[4] A. R. Hileman, *Insulation Coordination for Power Systems*. Boca Raton, FL, USA: CRC Press, 1999.

[5] E. Kuffel, W. S. Zaengl, and J. Kuffel, *High Voltage Engineering: Fundamentals*, 2nd ed. Oxford, U.K.: Newnes, 2000.

[6] J. Martínez, *Coordinación de aislamiento en redes eléctricas de alta tensión*. Madrid, Spain: McGraw-Hill, 2007.

[7] IEC 60071-1, Insulation Co-ordination—Part 1: Definitions, Principles and Rules. Geneva, Switzerland: International Electrotechnical Commission, 2019.

[8] IEC 60071-2, Insulation Co-ordination—Part 2: Application Guidelines. Geneva, Switzerland: International Electrotechnical Commission, 2018.

https://doi.org/10.14483/23448393.23305

[9] IEC TR 60071-4, Insulation Co-ordination—Part 4: Computational Guide to Insulation Co-ordination and Modelling of Electrical Networks. Geneva, Switzerland: International Electrotechnical Commission, 2004.

[10] IEC 60071-5, Insulation Co-ordination—Part 5: Procedures for High-Voltage Direct Current (HVDC) Converter Stations. Geneva, Switzerland: International Electrotechnical Commission, 2014.

[11] M. S. Naidu and V. Kamaraju, *High Voltage Engineering*. New York, NY, USA: McGraw-Hill, 1995.

[12] C. L. Wadhwa, *High Voltage Engineering*. New Delhi, India: New Age International (P) Ltd., 2007.

[13] Q. Wen *et al.*, "Lightning overvoltage identification in distribution line based on relevance vector machine," in *Proc. China Int. Conf. Electr. Distrib. (CICED)*, 2018, pp. 1206–1210. https://doi.org/10.1109/CICED.2018.8592419

[14] D. Lin, D. Bin, S. Wenxia, C. Weigen, and L. Jing, "Identifying the overvoltage in distribution networks based on support vector machine," in *Proc. Int. Conf. High Volt. Eng. Appl. (ICHVE)*, 2008, pp. 677–680. https://doi.org/10.1109/ICHVE.2008.4774025

[15] A. L. Antunes De Sa and R. A. Marshall, "Lightning Distance Estimation Using LF Lightning Radio Signals via Analytical and Machine-Learned Models," *IEEE Trans. Geosci. Remote Sens.*, vol. 58, no. 8, pp. 5892–5907, 2020. https://doi.org/10.1109/TGRS.2020.2972153

[16] H. Karami, A. Mostajabi, M. Azadifar, M. Rubinstein, C. Zhuang, and F. Rachidi, "Machine Learning-Based Lightning Localization Algorithm Using Lightning-Induced Voltages on Transmission Lines," *IEEE Trans. Electromagn. Compat.*, vol. 62, no. 6, pp. 2512–2519, 2020. https://doi.org/10.1109/TEMC.2020.2978429

[17] J. A. Martinez-Velasco, *Power System Transients: Parameter Determination*. Boca Raton, FL, USA: CRC Press/Taylor & Francis Group, 2010.

[18] L. Perdomo, A. Alfonso, F. Santamaria, and F. Roman, "Sensitivity Study of Induced Transient Overvoltages on Distribution Networks," in *Proc. 20th Int. Symp. High Voltage Eng. (ISH 2017)*, Buenos Aires, Argentina, 2017, pp. 1–6. [Online]. Available: https://www.e-cigre.org/publications/detail/ish2017-482-sensitivity-study-of-induced-transient-overvoltages-on-distribution-networks.html.

[19] V. Cooray, F. Rachidi, and M. Rubinstein, *Lightning Electromagnetics, vol. 1: Return Stroke Modelling and Electromagnetic Radiation*. London, U.K.: Institution of Engineering and Technology, 2022. https://doi.org/10.1049/PBPO127F

[20] V. Cooray, F. Rachidi, and M. Rubinstein, *Lightning Electromagnetics, vol. 2: Electrical Processes and Effects*. London, U.K.: Institution of Engineering and Technology, 2022. https://doi.org/10.1049/PBPO127G

[21] A. Piantini, *Lightning Interaction with Power Systems, vol. 1: Fundamentals and Modelling*. London, U.K.: Institution of Engineering and Technology, 2020. https://doi.org/10.1049/PBPO172F

https://doi.org/10.14483/23448393.23305

[22] A. Piantini, *Lightning Interaction with Power Systems, vol. 2: Applications*. London, U.K.: Institution of Engineering and Technology, 2020. https://doi.org/10.1049/PBPO172G

[23] Y. Baba and V. A. Rakov, *Lightning-Induced Effects in Electrical and Telecommunications Systems*. London, U.K.: Institution of Engineering and Technology, 2020. https://doi.org/10.1049/PBPO114E

[24] P. Chowdhuri, *Electromagnetic Transients in Power Systems*. Taunton, U.K.: John Wiley & Sons, Inc., 1996.

[25] L. E. Perdomo Orjuela, F. Santamaría, and F. Román, "Transient overvoltage in distribution networks in rural areas," in *Proc. 33rd Int. Conf. Lightning Protection (ICLP)*, Estoril, Portugal, 2016, pp. 1–6. https://doi.org/10.1109/ICLP.2016.7791433

[26] L. E. Perdomo Orjuela, F. Santamaría Piedrahita, and F. Román Campos, *Prototipo para el registro de sobretensiones transitorias estándar de 1.2/50 µs*, Master's thesis, Maestría en Ingeniería Eléctrica, Universidad Nacional de Colombia, Bogotá, Colombia, 2019. [Online]. Available: https://repositorio.unal.edu.co/handle/unal/69632

[27] L. Perdomo, A. Alfonso, and F. Santamaría, *Prototipo para el registro de sobretensiones transitorias en redes de tensión menor a 1 kV*. Bogotá, Colombia: Universidad Distrital Francisco José de Caldas, 2014.

[28] A. Alfonso, L. Perdomo, F. Santamaría, F. Amórtegui, and F. Román, "Integrity analysis of the signal transmitted to a 4G LTE module," in *Proc. Eur. Conf. Circuit Theory Design (ECCTD)*, Catania, Italy, 2017, pp. 1–4. https://doi.org/10.1109/ECCTD.2017.8093345

[29] L. Perdomo, A. Alfonso, F. Santamaría, and F. Román, "Development and Characterization of a Transient Overvoltage Recorder in Distribution Networks," in *Proc. 21st Int. Symp. High Voltage Eng. (ISH 2019)*. Cham, Switzerland: Springer, 2020, pp. 157–170. https://doi.org/10.1007/978-3-030-31676-1_16

[30] A. Alfonso, L. Perdomo, F. Santamaría, and C. Gómez, "Transient surges analysis in low voltage networks," *Tecnura*, vol. 18, no. Spec. Issue Doctorate, pp. 41–50, 2014. https://doi.org/10.14483/22487638.9241

[31] L. Li, R. Che, and H. Zang, "A fault cause identification methodology for transmission lines based on support vector machines," in *Proc. IEEE PES Asia-Pacific Power Energy Eng. Conf. (APPEEC)*, Xi'an, China, 2016, pp. 1430–1434. https://doi.org/10.1109/APPEEC.2016.7779725

[32] N. Harnzah, F. H. Anuwar, Z. Zakaria, and N. M. Tahir, "Classification of transient in power system using support vector machine," in *Proc. 5th Int. Colloq. Signal Process. Appl. (CSPA)*, Kuala Lumpur, Malaysia, 2009, pp. 418–422. https://doi.org/10.1109/CSPA.2009.5069263

[33] A. Adekitan and M. Rock, "Application of Machine Learning to Lightning Strike Probability Estimation," in *Proc. Int. Conf. Electr., Telecommun. Comput. Eng. (ICELTICs)*, Beirut, Lebanon, 2020, pp. 1–9. https://doi.org/10.1109/ICELTICs50595.2020.9315398

https://doi.org/10.14483/23448393.23305

[34] R. Tervo, J. Karjalainen, and A. Jung, “Short-Term Prediction of Electricity Outages Caused by Convective Storms,” *IEEE Trans. Geosci. Remote Sens.*, vol. 57, no. 11, pp. 8618–8626, 2019. https://doi.org/10.1109/TGRS.2019.2921809

[35] R. Tervo, J. Karjalainen, and A. Jung, “Predicting Electricity Outages Caused by Convective Storms,” in *Proc. IEEE Data Sci. Workshop (DSW)*, Lausanne, Switzerland, 2018, pp. 145–149. https://doi.org/10.1109/DSW.2018.8439906

[36] H. Torres Sánchez, *Protección contra rayos*. Bogotá, Colombia: Universidad Nacional de Colombia and ICONTEC, 2010.

[37] A. Küchler, *High Voltage Engineering: Fundamentals, Technology and Applications*. Berlin, Germany: Springer Vieweg, 2018. https://doi.org/10.1007/978-3-642-11993-4_7

[38] J. C. Das, *Transients in Electrical Systems: Analysis, Recognition, and Mitigation*. New York, NY, USA: McGraw-Hill, 2010.

[39] W. Hauschild and W. Mosch, *Statistical Techniques for High-Voltage Engineering*. London, U.K.: Institution of Engineering and Technology, 1992. https://doi.org/10.1049/PBPO013E

[40] R. E. Jaimes and Q. Su, *Condition Assessment of HV Insulation in Power System Equipment*. London, U.K.: Institution of Engineering and Technology, 2008. https://doi.org/10.1049/PBPO053E

[41] H. M. Ryan, *High-Voltage Engineering and Testing*. London, U.K.: Institution of Engineering and Technology, 2013. https://doi.org/10.1049/PBPO066E

[42] M. Brignone *et al*., “Lightning-Induced Voltages on Overhead Distribution Lines Computed through Analytical Expressions for the Electromagnetic Fields,” in *Proc. 35th Int. Conf. Lightning Protection (ICLP) and XVI Int. Symp. Lightning Protection (SIPDA)*, Colombo, Sri Lanka, 2021, pp. 1–6. https://doi.org/10.1109/ICLPandSIPDA54065.2021.9627387

[43] J. Guo, M. Rubinstein, V. Cooray, and F. Rachidi, “Lightning-Induced Voltage on an Overhead Transmission Line Terminated with Non-Vertical Risers,” in *Proc. 35th Int. Conf. Lightning Protection (ICLP) and XVI Int. Symp. Lightning Protection (SIPDA)*, Colombo, Sri Lanka, 2021. https://doi.org/10.1109/ICLPandSIPDA54065.2021.9627332

[44] A. Haddad and D. Warne, *Advances in High Voltage Engineering*, 2nd ed. London, U.K.: Institution of Engineering and Technology, 2004. https://doi.org/10.1049/PBPO040E

[45] K. Arreaza, “Curso de Especialización Coordinación de Aislamiento,” *Inel Engineering Education*. [Online]. Available: https://inelinc.com/curso/coordinacion-de-aislamiento-uwfam

[46] H. Rojas, L. Morales, and A. Santa, *Sistemas de medición indirecta de rayos*. Bogotá, Colombia: Universidad Distrital Francisco José de Caldas, 2026. https://doi.org/10.69740/UD.9789587879186.9789587879209

[47] L. Perdomo, A. Alfonso, B. Anillo, F. Santamaria, and N. Vera, “Classification of Direct Lightning Stroke According to Its Polarity in Medium Voltage Networks Based on Deep Learning Neural Networks,” in *Proc. 37th Int. Conf. Lightning Protection (ICLP)*, Dresden,

https://doi.org/10.14483/23448393.23305

Germany, 2024, pp. 932–937. [Online]. Available: https://ieeexplore.ieee.org/document/10832625

[48] K. Arreaza and J. Videla, “Curso de Especialización Cálculos Avanzados en Líneas de Transmisión,” *Inel Engineering Education*. [Online]. Available: https://inelinc.com/curso/calculos-avanzados-en-lineas-de-transmision-btwlx

[49] IEEE Power and Energy Society Substations Committee, *IEEE Guide for Direct Lightning Stroke Shielding of Substations*. New York, NY, USA: Institute of Electrical and Electronics Engineers, 2012. [Online]. Available: https://standards.ieee.org/ieee/998/1376/

[50] IEEE Power and Energy Society Transmission and Distribution Committee, *IEEE Guide for Improving the Lightning Performance of Transmission Lines*. New York, NY, USA: Institute of Electrical and Electronics Engineers, 1997. [Online]. Available: https://standards.ieee.org/ieee/1243/1891/

[51] IEEE Power and Energy Society Transmission and Distribution Committee, *IEEE Guide for Improving the Lightning Performance of Electric Power Overhead Distribution Lines*. New York, NY, USA: Institute of Electrical and Electronics Engineers, 2011. [Online]. https://standards.ieee.org/ieee/1410/4720/

[52] S. Hernández, “Inteligencia Artificial y Deep Learning desde Cero en Python,” *Udemy*. [Online]. https://www.udemy.com/course/deep-learning-desde-cero-en-python

[53] IEEE Power and Energy Society Transmission and Distribution Committee, *IEEE Guide for Electric Power Distribution Reliability Indices (IEEE Std 1366-2012)*. New York, NY, USA: Institute of Electrical and Electronics Engineers, 2012. [Online]. https://standards.ieee.org/ieee/1366/4602/

[54] E. Gonzalez, F. Jurado, G. Jose, and M. Julio, “Extreme testing of guard cables with fiber optics: A case study,” *Ingeniería*, vol. 29, no. 3, p. 21, 2024. https://doi.org/10.14483/23448393.21483

[55] A. Mishra, “Signal Integrity Basics to Advanced & Simulations – EsteemPCB,” *Udemy*. [Online]. https://www.udemy.com/course/signal-integrity-basics-to-advanced-simulations-esteempcb

[56] P. Jiménez, “Programa de Especialización Parametrización, Configuración y Operación de Relés ABB,” *Inel Engineering Education*. [Online]. https://inelinc.com/curso/programa-especializacion-parametrizacion-configuracion-operacion-reles-abb-hitachi-u6i6y

[57] P. Jiménez, “Programa de Especialización Parametrización, Configuración y Operación de Relés General Electric,” *Inel Engineering Education*. [Online]. https://inelinc.com/curso/programa-de-especializacion-parametrizacion-configuracion-y-operacion-de-reles-general-electric-6ylkr

[58] A. T. Johns and S. K. Salman, *Digital Protection for Power Systems*. London, U.K.: Institution of Electrical Engineers, 2022.

[59] *Criterios Generales de Protección de los Sistemas Eléctricos Insulares y Extrapeninsulares*. Madrid, Spain: ENDESA–Red Eléctrica de España (REE), 2005.

[60] Comité de Operación Económica del Sistema Interconectado Nacional (COES), *Criterios de Ajuste y Coordinación de los Sistemas de Protección del SEIN*. Lima, Perú: COES-SINAC, 2022.

[61] A. G. Phadke and J. S. Thorp, *Computer Relaying for Power Systems*. Chichester, U.K.: John Wiley & Sons, 2009. https://doi.org/10.1002/9780470749722

[62] IEEE Power System Relaying and Control Committee, *IEEE Standard Inverse-Time Characteristic Equations for Overcurrent Relays (IEEE Std C37.112-2018)*. New York, NY, USA: Institute of Electrical and Electronics Engineers, 2019. [Online]. https://standards.ieee.org/ieee/C37.112/7036/

[63] A. R. van C. Warrington, *Protective Relays: Their Theory and Practice*. Norwich, U.K.: Chapman & Hall Ltd., 1968.

[64] J. M. Gers and E. J. Holmes, *Protection of Electricity Distribution Networks*. London, U.K.: Institution of Engineering and Technology, 2022. https://doi.org/10.1049/PBPO180E

[65] R. Mason, *The Art and Science of Protective Relaying*. General Electric.

[66] S. H. Horowitz, A. G. Phadke, and J. K. Niemira, *Power System Relaying*. Chichester, U.K.: John Wiley & Sons, 2013.

[67] H. L. Willis and M. H. Rashid, *Protective Relaying: Principles and Applications*. Boca Raton, FL, USA: CRC Press/Taylor & Francis Group, 2006.

[68] W. A. Elmore, *Protective Relaying: Theory and Applications*. New York, NY, USA: Marcel Dekker, Inc., 2004.

[69] Q. Wu, Z. Lu, and T. Ji, *Protective Relaying of Power Systems Using Mathematical Morphology*. London, U.K.: Springer, 2009.

[70] P. M. Anderson and P. Rush, *Network Protection and Automation Guide*. Barcelona, Spain: AREVA T&D Automation & Information Systems, 2005.

[71] P. M. Anderson, *Power System Protection*. New York, NY, USA: Institute of Electrical and Electronics Engineers, 1999.

[72] IEEE Industry Applications Society Industrial and Commercial Power Systems Department Committee, *IEEE Recommended Practice for Protection and Coordination of Industrial and Commercial Power Systems*. New York, NY, USA: Institute of Electrical and Electronics Engineers, 2001. [Online]. https://standards.ieee.org/ieee/242/426

[73] J. D. McDonald, *Electric Power Substations Engineering*. Boca Raton, FL, USA: CRC Press, 2012.

[74] A. M. Sleva, *Protective Relay Principles*. Boca Raton, FL, USA: CRC Press, 2009.

[75] K. Arreaza, “Curso de Especialización Automatización de Subestaciones IEC 61850,” *Inel Engineering Education*. [Online]. https://inelinc.com/curso/automatizacion-de-subestaciones-iec-61850-l9kaf

[76] P. B. Nair and Nirmal-Kumar C., *IEC 61850: Principles and Applications to Electric Power Systems*. 2023.

https://doi.org/10.14483/23448393.23305

[77] Y. Yuan and Y. Yang, *IEC 61850-Based Smart Substations: Principles, Testing, Operation and Maintenance*. Beijing, China: China Electric Power Press, 2019.

[78] A. Apostolov, *IEC 61850: Digitizing the Electric Power Grid*. Norwood, MA, USA: Artech House, 2023.

[79] M. S. Thomas and J. D. McDonald, *Power System SCADA and Smart Grids*. Boca Raton, FL, USA: CRC Press, 2015.

[80] J. Luo, Y. Hao, Q. Ye, Y. Hao, and L. Li, "Development of Optical Fiber Sensors Based on Brillouin Scattering and FBG for On-Line Monitoring in Overhead Transmission Lines," *J. Lightwave Technol.*, vol. 31, no. 10, pp. 1559–1565, 2013. https://doi.org/10.1109/JLT.2013.2252882

[81] G. Ma, C. Li, J. Quan, J. Jiang, and Y. Cheng, "A Fiber Bragg Grating Tension and Tilt Sensor Applied to Icing Monitoring on Overhead Transmission Lines," *IEEE Trans. Power Deliv.*, vol. 26, no. 4, pp. 2163–2170, 2011. https://doi.org/10.1109/TPWRD.2011.2157947

[82] K. T. V. Grattan and T. Sun, "Fiber Optic Sensor Technology: An Overview," *Sens. Actuators A Phys.*, vol. 82, nos. 1–3, pp. 40–61, 2000. https://doi.org/10.1016/S0924-4247(99)00368-4

[83] K. Fidanboylu and H. Efendioğlu, "Fiber Optic Sensors and Their Applications," in *Proc. 5th Int. Adv. Technol. Symp. (IATS'09)*, Karabük, Turkey, 2009.

[84] K. Zhang and D. Li, *Electromagnetic Theory for Microwaves and Optoelectronics*. Beijing, China: Springer, 2008.

[85] F. Rachidi and S. Tkachenko, *Electromagnetic Field Interaction with Transmission Lines: From Classical Theory to HF Radiation Effects*. Southampton, U.K.: WIT Press, 2008. https://doi.org/10.2495/978-1-84564-063-7

## Authors and biographies

**Luis Eduardo Perdomo Orjuela** received a BSc degree in Electrical Engineering from Universidad Distrital Francisco José de Caldas in 2014 and subsequently earned a MSc degree in Electrical Engineering from Universidad Nacional de Colombia in 2019. He is currently pursuing a second MSc in Information and Communication Sciences at Universidad Distrital Francisco José de Caldas. With more than ten years of professional experience in the electrical, electronics, and ICT sectors, he has developed advanced expertise in the maintenance of medium- and high-voltage substations, digital substations, protection and control systems, and data analytics, among other areas. In this role, he has been responsible for ensuring the reliability and operational integrity of power systems, in addition to managing maintenance activities in power, control, protection and digital substations. He has also verified power system designs, including substations and transmission lines. He currently works at Ingeniería y Soluciones Especializadas (ISES), performing factory acceptance tests (FAT), site acceptance tests (SAT), system integration tests (SIT), stability tests, and functional tests, as part of witness testing and commissioning activities for substation control, protection, and telecommunications systems, among other technical evaluations.

Email: leperdomoo@unal.edu.co, leperdomoo@udistrital.edu.co.

https://doi.org/10.14483/23448393.23305

**Francisco Santamaria Piedrahita** received his BSc, MSc, and PhD degrees in Electrical Engineering from Universidad Nacional de Colombia in 2002, 2007, and 2013. In 2010 he joined the staff of the Department of Electrical Engineering at Universidad Distrital Francisco Jose de Caldas, where he currently works as a full professor and member of the research group on Electrical Systems and Energy Efficiency (GISE3). His research interests include lightning protection, electromagnetic interference, electric vehicles, and energy management systems.

Email: fsantamariap@udistrital.edu.co

**Nelson Enrique Vera Parra** is a full professor and former head of the Research Office of the Universidad Distrital Francisco José de Caldas. He is an Electronics Engineer with an MSc in Information and Communication Sciences and a PhD in Engineering. He also serves as a researcher in the GICOGE group (International Group in Computing and Communications for Knowledge Management), focusing on high-performance computing, data science, artificial intelligence, and bioinformatics.

Email: neverap@udistrital.edu.co